Dalton Transactions

ROYAL SOCIETY OF CHEMISTRY

PAPER

View Article Online
View Journal | View Issue

Cite this: *Dalton Trans.*, 2025, **54**, 13950

Redox-active inverse crowns – pockets for heavier chalcogenides

Johannes Maurer, Lukas Klerner, Jens Langer and Sjoerd Harder *

Received 8th August 2025,
Accepted 2nd September 2025

DOI: 10.1039/d5dt01896j

rsc.li/dalton

The reactivity of the redox-active metal crown complex (BDI*)$MgNa_3N''_2$ (**VI**), formally containing a Mg^0 centre, with phosphine chalcogenides, $R_3P{=}Ch$ (Ch = O, S, Se, Te; R = Me, Et) was investigated (BDI* = $HC[tBuC{=}N(DIPeP)]_2$ with DIPeP = 2,6-Et_2CH-phenyl). While all $R_3P{=}Ch$ reagents could be reduced, only the heavier ones led to clean reduction to S^{2-}, Se^{2-} and Te^{2-} anions which were captured in the metalla-cycle. The smaller S^{2-} anion can be stabilized by the tetrametallic $MgNa_3$-crown but the larger Se^{2-} and Te^{2-} require a pentametallic $MgNa_4$-crown. Reaction of the sulfide complex with N_2O led to a rare thiohyponitrite *cis*-$SNNO^{2-}$ anion which is trapped in the pentametallic $MgNa_4$-crown. Experimental observations and bonding characteristics of all complexes are supported by an additional computational study.

Introduction

Classic crown ethers like 18-crown-6 developed by Pedersen effectively bind metal cations within their polyether cavity (**I**, Scheme 1a – top).[1–3] In contrast, inverse crown ethers inverse this concept and trap anions within a cavity spanned by metal cations (**II**, Scheme 1a – bottom). Seminal reports by Mulvey and coworkers describe the serendipitous self-assembly of inverse crown ethers by reaction of Na^{n}Bu, Mg(^{n}Bu)$_2$ and HN″ (N″ = $[N(SiMe_3)_2]^-$) and small quantities of oxygen impurities like O_2 or H_2O.[4,5] Such complexes are generally formed in low yields and often mixtures of oxides and peroxides are obtained. These initial investigations have been extended to capturing more complex moieties within the metal crown, enabling the synthesis of unique multi-anionic products that are not accessible by standard deprotonation methods.[6]

Although the first inverse crown ethers with O^{2-} core anions have been extensively investigated, similar metal crown complexes with heavier chalcogenide anions (S^{2-}, Se^{2-}, Te^{2-}) have so far not been reported. There is in general a lack of information on polar *s*-block metal complexes with heavy chalcogenides. The Cambridge Crystallographic Database contains only three crystal structures of *s*-block metal complexes with sulfide anions, *i.e.* complex **III**-S (Scheme 1b) and solvates thereof.[7,8] For polar selenide complexes there are only two examples, **III**-Se and the scorpionate complex **IV** (Scheme 1b).[8,9] *s*-Block metal complexes with encapsulated Te^{2-} anions are completely unknown. There are rare reports for the more polar molecular aluminium complexes with heavier chalcogenide anions (*e.g.* **V**-Ch, Scheme 1b).[10–12] This lack of knowledge stands in strong contrast with transition metal chalcogenide chemistry for which complexes[13–22] and materials[23] have been well studied.

Herein, we present a unique "reduce-and-capture" concept to access ionic *s*-block metal complexes of the heavier chalcogenides Ch^{2-} anions. We recently introduced a redox-active metal crown complex (**VI**, Scheme 1c) that is able to reduce a substrate and encapsulate the resulting dianion.[24] This was exemplary shown for reaction with N_2O or epoxides, producing the O^{2-} anion, or for reaction with O_2 to give an encapsulated peroxide dianion. Depending on stoichiometry, reactions with S_8 resulted either in reduction to S^{2-} or formation of S_2^{2-}. Herein, we extend these investigations aiming to isolate complexes with a Se^{2-} anion, which are rare, or a Te^{2-} anion, which are hitherto unknown. As the ionic radii of the Ch^{2-} dianions gradually increase from O^{2-} (1.40 Å) over S^{2-} (1.84 Å) and Se^{2-} (1.98 Å) to Te^{2-} (2.21 Å) by almost 58%,[25] we were particularly interested whether capturing these larger anions requires ring extension. We also discuss trends in crystal structures, discuss solution dynamics and support our findings with DFT calculations.

Results and discussion

Phosphine chalcogenides, $R_3P{=}Ch$, have been shown to be potent chalcogen transferring agents.[8,10–12,26–32] The key to this reactivity lies within the P=Ch bond which strictly speaking has more ylid (P^+–Ch^-) than ylene character and weakens

Inorganic and Organometallic Chemistry, Friedrich-Alexander-Universität Erlangen-Nürnberg, Egerlandstraße 1, 91058 Erlangen, Germany.
E-mail: sjoerd.harder@fau.de

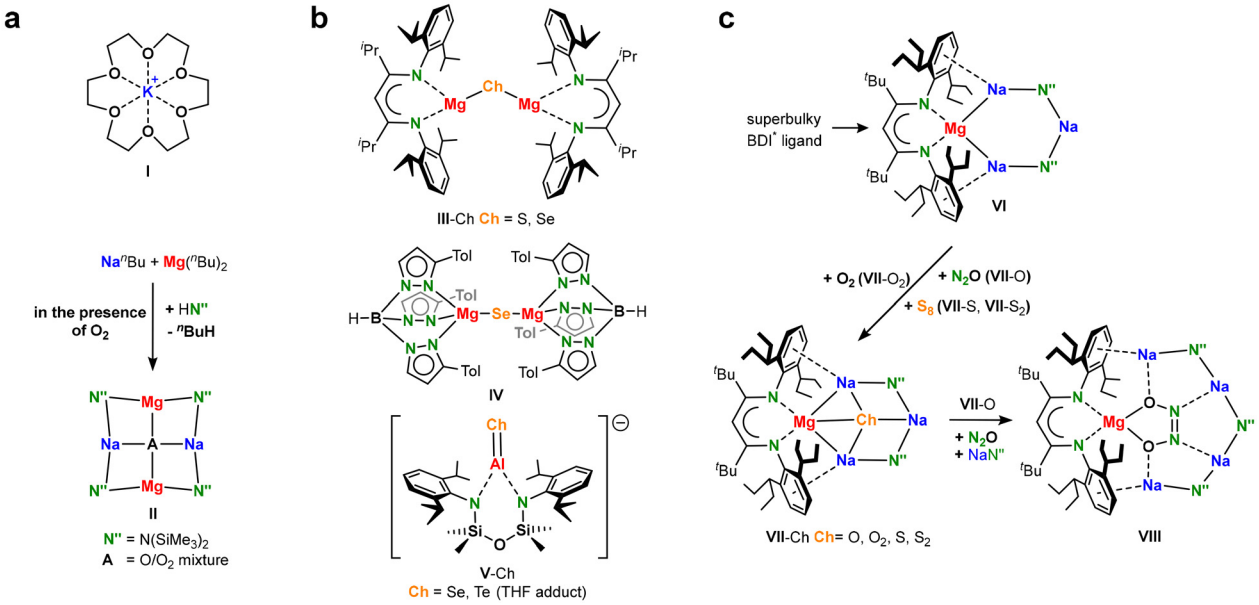

Scheme 1 (a) From Pedersen's crown ethers[1–3] to Mulvey's inverse crown complexes.[4–6] (b) Main group metal complexes with formal Ch^{-II} centres.[8–11] (c) The reduction of O_2, N_2O or S_8 with redox-active metal crown complex VI.[24]

going down group 16 (P=O: 130 kcal mol^{-1}, P=S: 81 kcal mol^{-1}, P=Se: 64 kcal mol^{-1}, P=Te: 44 kcal mol^{-1}).[33] Consequently, reduction of R_3P=Ch to the respective R_3P and Ch^{2-} fragments becomes easier along the row Ch = O < S < Se < Te.

Use of Ph_3P=Ch reagents has been shown to be problematic in chalcogenide anion generation. The side-product PPh_3 cannot be separated easily from the reaction mixture, culminating in a drastic decrease of isolated product yields.[8] Taking this into account, we chose to use Me_3P=Ch and Et_3P=Ch which have the advantage to produce volatile PMe_3 and PEt_3 which can be easily removed under vacuum. In all cases (Ch = O, S, Se, Te), DFT calculations support the thermodynamic feasibility for the formation of (BDI*)$MgNa_3N''_2$(Ch) from **VI** and Me_3P=Ch (Scheme 2). The reaction with Me_3P=O is the least exothermic while the reductions of the heavier phosphine chalcogenides release nearly double this energy.

In a general procedure, a solution of the redox-active metal crown complex (BDI*)$MgNa_3N''_2$ (**VI**) in cyclohexane-d_{12} was reacted with one equivalent of Me_3P=Ch (or Et_3P=Ch) at room temperature. Upon stirring, the dark red colour of the reaction mixtures usually turned to yellow, indicative of Mg^0 to Mg^{+II} conversion. The volatiles, including the phosphine side-product, were removed under high vacuum and the selectivity of the reaction was checked by ^{1}H NMR.

Formation and trapping of the oxide dianion (VII-O)

Whereas the reduction of N_2O with **VI** is facile and cleanly produced (BDI*)$MgNa_3N''_2$(O) (**VII**-O), the reaction of **VI** with one equivalent of Me_3P=O only led to 33% conversion. The other 66% of **VI** remained untouched. Addition of two more equivalents of Me_3P=O finally led to full conversion of **VI** into one major, yet unknown product, which according to ^{1}H NMR chemical shifts is not the expected (BDI*)$MgNa_3N''_2$(O) (**VII**-O). The observed proton spectrum is identical to that of the product formed in reaction of $[(BDI^*)Mg]_2Na_2$ with two equivalents of Me_3P=O (SI Fig. S50). This indicates that upon addition of Me_3P=O the inverse crown template **VI** dis-

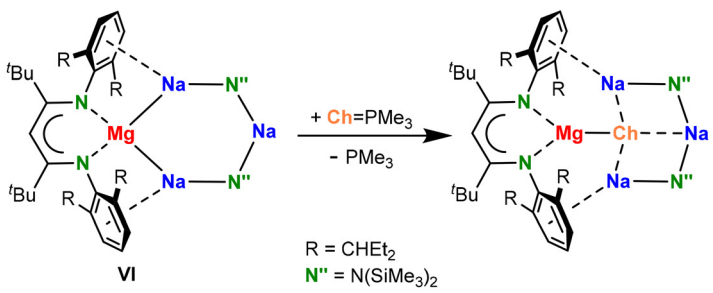

Ch	ΔH	ΔG_{298K}
O	-37.0	-33.6
S	-62.7	-64.4
Se	-64.9	-65.7
Te	-63.0	-62.4

(in kcal mol^{-1})

Scheme 2 Calculated reaction enthalpies and free energies (kcal mol^{-1}; B3PW91-GD3BJ/def2tzvp//B3PW91-GD3BJ/def2svp) for reaction of VI with Me_3P=Ch to metal crown complexes of the Ch^{2-} anions.

assembled and decomposed in $[(BDI^*)Mg]_2Na_2$ and NaN″ (Scheme 3). This is supported by NMR spectroscopy and X-ray diffraction analysis which are consistent with formation of $[(NaN'')(Me_3P{=}O)]_2$ (SI, Fig. S55). We earlier reported that **VI** disintegrates when dissolved in polar solvents as for example THF. Like THF, $Me_3P{=}O$ can act like a polar solvent, resulting in disassembly of **VI** and isolation of $[(NaN'')(Me_3P{=}O)]_2$.

Formation and trapping of the sulfide dianion (VII-S)

Exchange of $Me_3P{=}O$ for the much less polar phoshine sulfide reagent, $Me_3P{=}S$, led to clean oxidation of **VI** and exclusive formation of $(BDI^*)MgNa_3N''_2(S)$ (**VII**-S) and PMe_3 (Scheme 3). Removing the solvent and phosphine under high vacuum gave a quantitative yield of essentially pure **VII**-S without the need of any further purification steps. Quantitative formation of the sulfide complex stands in contrast with the modest yields reported for the reduction of Mg^I complexes with $Ph_3P{=}S$.[8] Clean reactivity to **VII**-S can be explained by the stabilizing influence of the metal crown. In addition, $Me_3P{=}S$ is much less polar than $Me_3P{=}O$ and not able to destroy the metal crown by coordination.

The oxidation of Mg^0 in **VI** with $Me_3P{=}S$ is the privileged route for the generation of the sulfide complex **VII**-S. In the previously reported procedure,[24] it was found critical to react **VI** with exactly 0.125 equivalents of S_8 at low temperatures and at high dilution in order to prevent the formation of the persulfide complex $(BDI^*)MgNa_3N''_2(S_2)$ (**VII**-S_2). Especially on a smaller scale, it was found difficult to exactly add stoichiometric quantities of sulfur. The current synthetic route can be conveniently carried out in cyclohexane at room temperature using an excess of $Me_3P{=}S$. Any unreacted $Me_3P{=}S$ remains as an insoluble solid which can be simply removed from the soluble product **VII**-S by filtration.

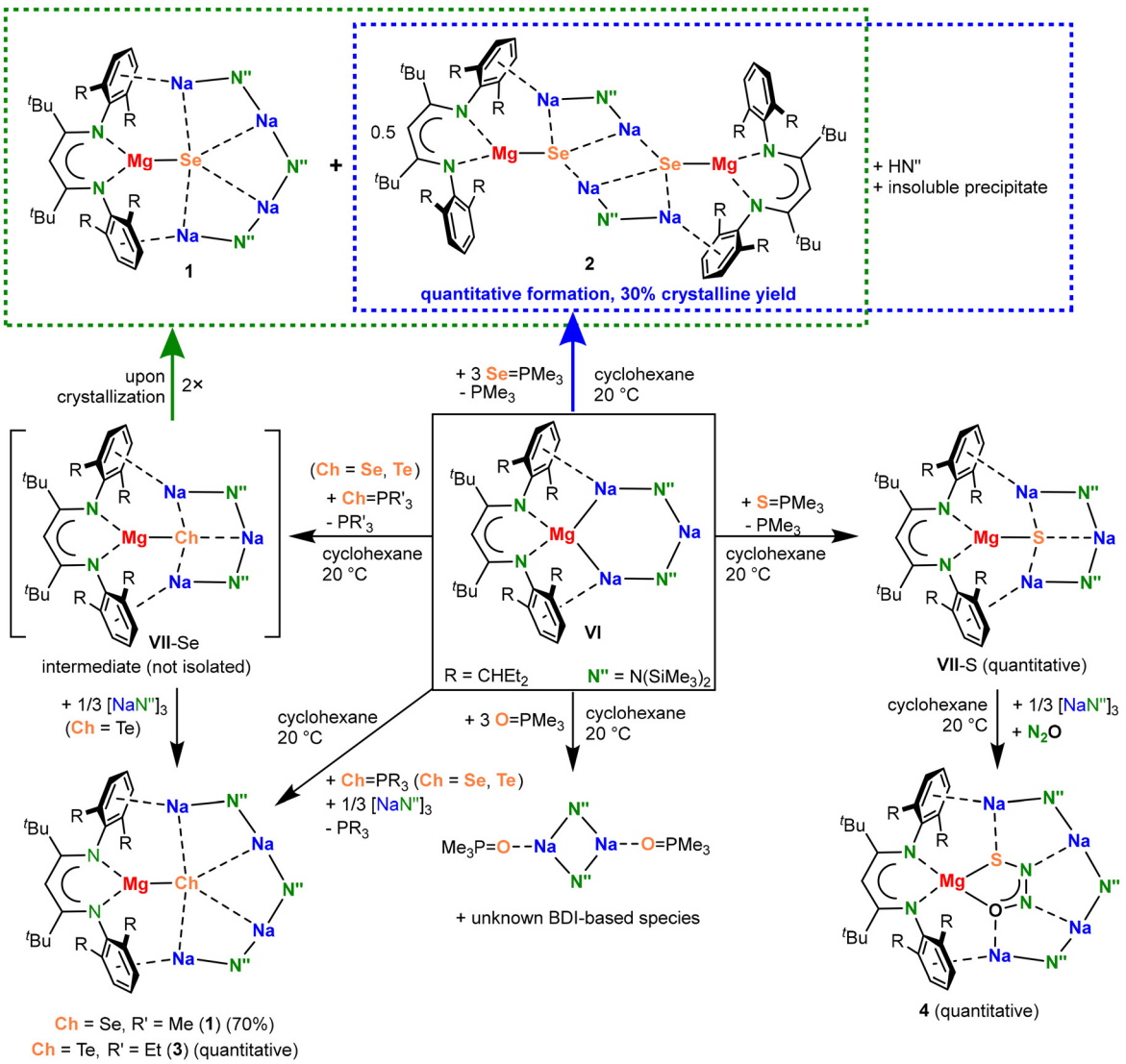

Scheme 3 Reactivity of VI with phosphine chalcogenides $Ch{=}PMe_3$ (Ch = O, S, Se) and $Te{=}PEt_3$.

Formation and trapping of the selenide and telluride dianions (1, 2, 3)

As $R_3P{=}Se$ and $R_3P{=}Te$ are both even less polar than $R_3P{=}S$ and the P=Se and P=Te bonds are weaker than the P=S bond, controlled reduction of these reagents with **VI** should be straightforward.

The reduction of $Me_3P{=}Se$ with **VI** led to the formation of various species among which complexes **1** and **2** are the main Mg selenide products (Scheme 3; raw product: Fig. S24 and S25). We presume that in a first step the expected product **VII**-Se is formed. However, in contrast to O^{2-} and S^{2-}, the Se^{2-} dianion is too large to comfortably fit in the (BDI*)$MgNa_3N''_2$ crown. Concentrating and cooling the mother liquor led to crystallization of a ring enlargement product in which an additional NaN″ is build in the ring: (BDI*)$MgNa_4N''_3$(Se) (**1**). Consequently, also a ring shrinkage product was found (BDI*)$MgNa_2N''$(Se) which crystallised as a dimer (**2**). As **1** and **2** are both well soluble in alkanes, purification by crystallization and washing procedures only resulted in very low yields. However, as shown in the synthesis of (BDI*)$MgNa_4N''_3$(ONNO) (**VIII**), ring expansion can be easily achieved by addition of 0.33 equivalents of trimeric $(NaN'')_3$ to the reaction mixture.[24] Using the same approach, complex **1** could be isolated as a pure compound in 70% crystalline yield. We also observed that using a three-fold excess of $Me_3P{=}Se$, **VI** reacts selectively to **2**, the complex depleted of NaN″, which could be crystallized in 30% yield. This may be explained by the observation that $(NaN'')_3$ itself also reacts with $Me_3P{=}Se$ to give a highly insoluble white solid (likely Na_2Se_2) and HN″ in which the origin of the proton remains unexplained. Using excess $Me_3P{=}Se$ thus removes NaN″ from **VI**, resulting in more selective formation of **2** which is depleted by one NaN″ unit. Thus, also complex **2** could be obtained pure and was after crystallization isolated in 30% yield. Complexes **1** and **2** both exhibit ^{77}Se NMR signals with highly negative chemical shifts (**1**: −821.8 ppm, **2**: −828.3 ppm; referenced to $SeMe_2$ as 0 ppm). These signals are considerably highfield-shifted when compared to Stasch's magnesium selenide complex **III**-Se (−764 ppm).[8] Complex **1** should show two different ^1H NMR signals in a 2 : 1 ratio for the unequal N″ ligands. The appearance of one signal indicates fast exchange between these ligands. At −70 °C the signal broadens but decoalescence is not reached (Fig. S12).

In case of Te, we used $Et_3P{=}Te$ as a reagent. The phosphine telluride $Me_3P{=}Te$ is relatively unstable and easily decomposes to Me_3P and elemental Te. In contrast, the bulkier $Et_3P{=}Te$ shows enhanced stability and PEt_3, which upon reduction is formed as a side-product, is still volatile enough for convenient removal under high vacuum. Reduction of $Et_3P{=}Te$ with **VI** led to the isolation of the ring extension product (BDI*)$MgNa_4N''_3$(Te) (**3**, Scheme 3). In this case, the ring shrinkage product could not be isolated or identified, probably due to poor stability. As discussed above, addition of 0.33 equivalent of trimeric $(NaN'')_3$ at the start of the experiment, led to clean formation of the extended ring product and **3** could now be isolated in essentially quantitative yield. Similarly to the NMR shifts observed for the central Se^{2-} cores in **1** and **2**, the ^{125}Te NMR spectrum of **3** features a noticeable high-field shifted resonance at −1902.3 ppm (referenced to $TeMe_2$ as 0 ppm). Depending on the substituents, TeR_2 compounds generally show ^{125}Te resonances between 0 and 500 ppm. The very negative chemical shift measured for **3** is also *circa* 500 to 1000 ppm more upfield than aluminium based tellurides with both single and double bonded Al–Te moieties.[12,34] Complex **3** should show two different ^1H NMR signals in a 2 : 1 ratio for the unequal N″ ligands. The appearance of one signal indicates fast exchange between these ligands. At −70 °C the signal broadens but decoalescence is not reached (Fig. S37).

These investigations show that for the smaller chalcogenides, O^{2-} and S^{2-}, the optimal ring size is defined by a tetrametallic $MgNa_3$-crown. The larger chalcogenides, Se^{2-} and Te^{2-}, require the extended pentametallic $MgNa_4$-crown. DFT calculations, concerning such ring extension show that O^{2-} encapsulation indeed prefers the smaller ring (Scheme 4 and Fig. S56) whereas the free energy difference for S^{2-} encapsulation in a small or large ring is close to zero. Ring extension for the larger anions, Se^{2-} and Te^{2-}, becomes more exergonic with increasing anion size.

Reactivity of metal crown chalcogenide complexes with N_2O

Inspired by the ring extension from a $MgNa_3$-ring in (BDI*)$MgNa_3N''_2$(O) (**VII**-O) to the $MgNa_4$-ring in the hyponitrite complex (BDI*)$MgNa_4N''_3$(ONNO) (**VIII**) (Scheme 1),[24] com-

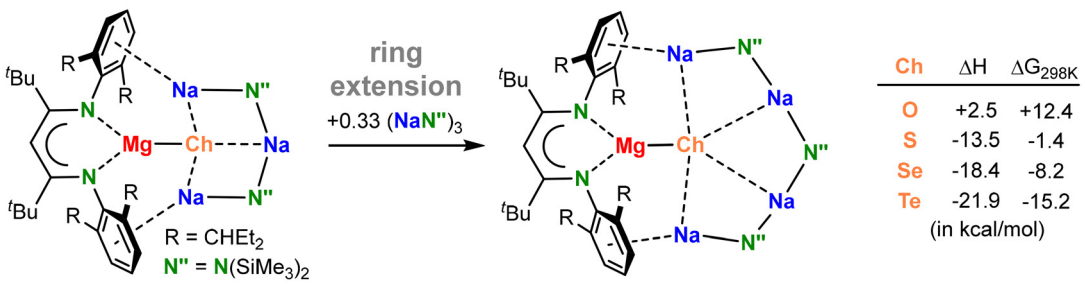

Ch	ΔH	ΔG_{298K}
O	+2.5	+12.4
S	-13.5	-1.4
Se	-18.4	-8.2
Te	-21.9	-15.2

(in kcal/mol)

Scheme 4 Calculated reaction enthalpies and free energies (kcal mol^{-1}; B3PW91-GD3BJ/def2tzvp//B3PW91-GD3BJ/def2svp) for ring extension by addition of 0.33 equivalent of $(NaN'')_3$.

plexes **VII**-S, **1** and **3** were exposed to an N_2O atmosphere. In all three cases, the ^{1}H NMR spectra showed complete conversion of the reactants, but only for **VII**-S quantitative formation of the thiohyponitrite complex (BDI*)$MgNa_4N''_3$(SNNO) (**4**) was observed. Reaction of **1** and **3** with N_2O led to mixtures containing a myriad of products which could not be further isolated or identified. Complex **4** is a rare thiohyponitrite complex and the first isolated complex with a *cis*-$SNNO^{2-}$ dianion trapped exclusively by main group metal cations.[35,36] Complex **4** should show three different ^{1}H NMR signals in a 1 : 1 : 1 ratio for the unequal N″ ligands. The appearance of one signal indicates fast exchange between these ligands. At −70 °C decoalescence is reached (Fig. S45).

Crystal structures

Complex **1** crystallized C_2-symmetric with the two-fold symmetry axis through the ligand backbone-CH, Mg, Se and one of the amide N atoms (Fig. 1a). The analogous Te complex **3** is approximately C_2-symmetric but does not possess crystallographic symmetry (Fig. 1b). The common feature of both compounds is the eight-membered Mg–Na–N–Na–N–Na–N–Na ring encapsulating the Ch^{2-} dianion. In contrast to **VI** in which the ring is held together by Mg–Na and Na–N bonds, the rings in **1** and **3** are formed by Ar···Na and Na–N bonding. While the Mg–Na bonds in **VI** are in the range of 3.261(2)–3.407(2) Å, the non-bonding Mg···Na1 distances in **1** measure 3.6568(6) Å. Those in **3** are slightly longer: 3.896(1)–3.951(1) Å. The latter lie within the range of the expanded metal crown complex **VIII** (Mg···Na 3.927(1)–3.965(1) Å). The Ar(centroid)···Na contacts in **1** and **3** vary from 2.625(1) to 2.705(1) Å and are of comparable length as similar interactions in **VI** (2.626(2)–2.735(2) Å) or **VIII** (2.600(1)–2.639(1) Å).[24]

The Mg–Ch bonds of 2.4141(6) Å in **1** and 2.6068(6) Å in **3** are much shorter than the comparable Na–Ch distances varying from 2.8792(5) to 3.0084(6) Å in **1** or 3.0629(8) to 3.2259(8) Å in **3**. The Mg–Ch bonds in **1** and **3** are also shorter

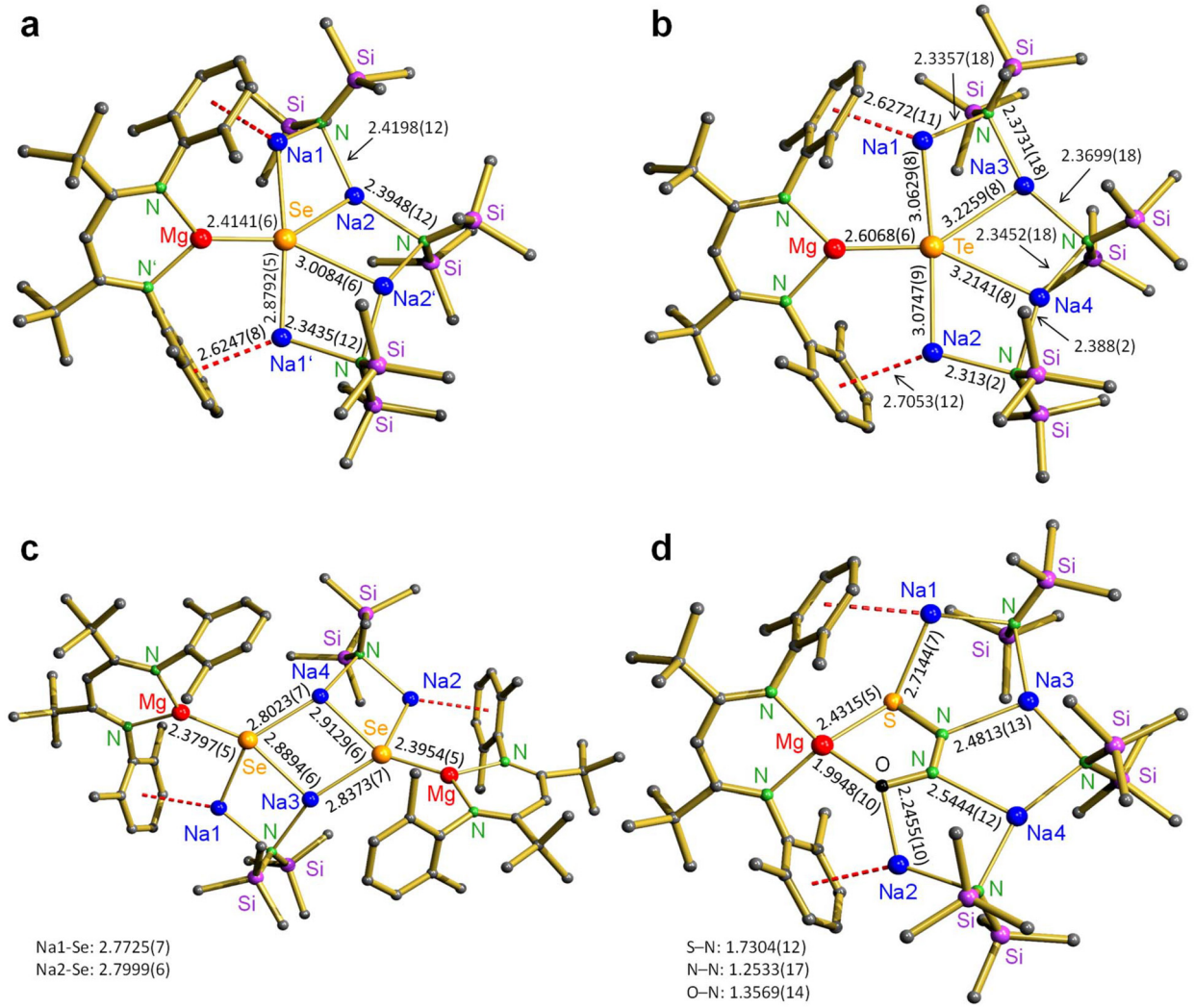

Fig. 1 Crystal structures; Et groups of the Et_2CH-substituents and H atoms are not shown for clarity. Bond distances shown in Å. (a) (BDI*)$MgNa_4N''_3$(Se) (**1**). (b) (BDI*)$MgNa_4N''_3$(Te) (**3**). (c) [(BDI*)$MgNa_2N''$(Se)]$_2$ (**2**). (d) (BDI*)$MgNa_4N''_3$(SNNO) (**4**).

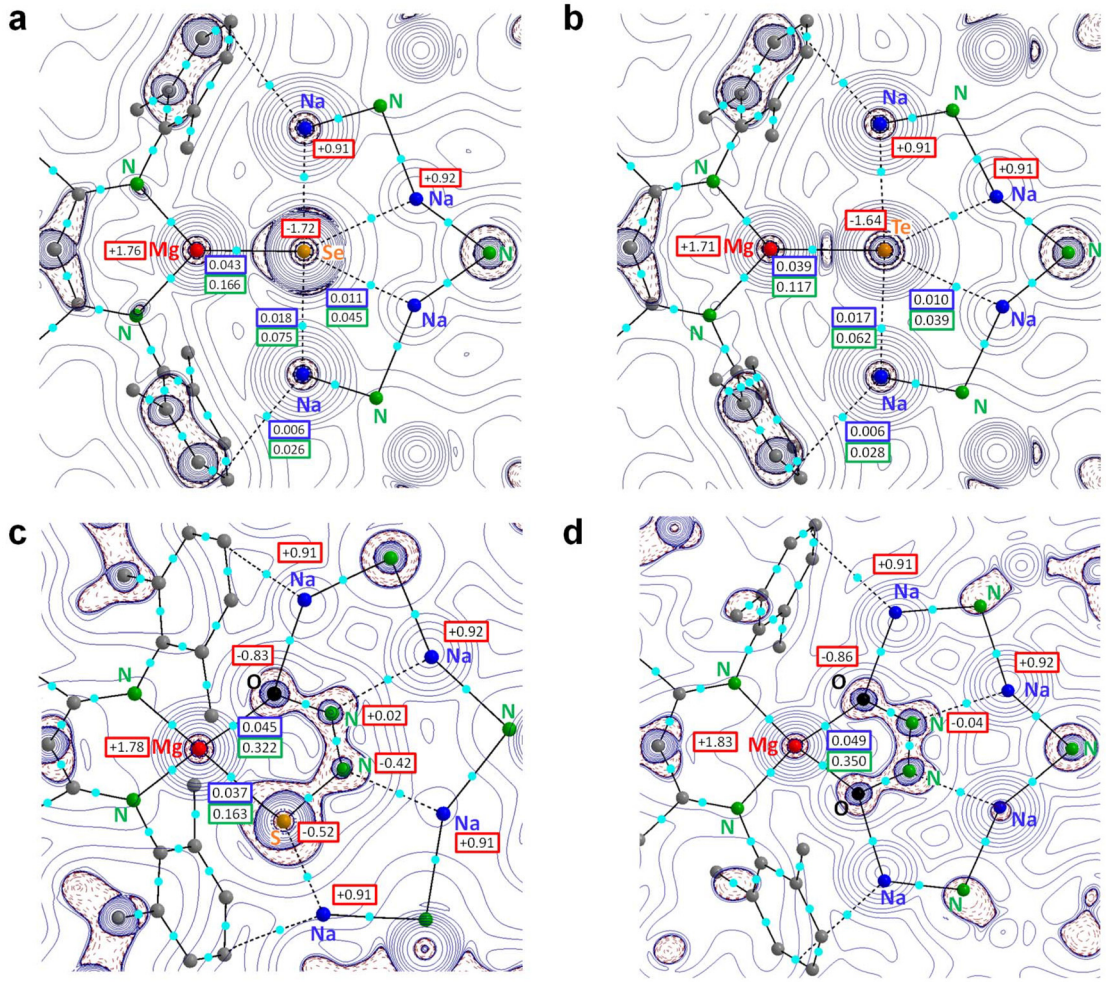

Fig. 2 NPA and Atoms-In-Molecules analyses. The Laplacian distributions show bcp's (light-blue) with $\rho(\mathbf{r})$ (e B^{-3} in blue boxes), the Laplacian $\nabla^2\rho(\mathbf{r})$ (e B^{-5} in green boxes) and NPA charges (red boxes). (a) (BDI*)$MgNa_4N''_3$(Se) (**1**). (b) (BDI*)$MgNa_4N''_3$(Te) (**3**). (c) (BDI*)$MgNa_4N''_3$(SNNO) (**4**). (d) (BDI*)$MgNa_4N''_3$(ONNO) (**VIII**).

than the sum of the covalence radii for Mg and Ch (Mg + Se: 2.61 Å, Mg + Te: 2.79 Å).[37] Mg–Se distances of similar length are observed in Parkin's magnesium selenide complex **IV** (2.404(3) and 2.408(3) Å)[9] and Stasch's **III**-Se (2.3497(18)–2.4739(18) Å).[8] The hitherto only compound with a Mg–Te bond that is crystallographically characterized, $Mg[TeSi(SiMe_3)_3]_2(THF)_2$, features considerably longer contacts (2.714(1)–2.720(2) Å) than in **3**.[38,39] This is likely due to the mono-anionic nature of $(Me_3Si)_3SiTe^-$ compared to dianionic Te^{2-}.

Complex **2** can be considered a dimer of (BDI*)$MgNa_2N''$(Se) units in which Se^{2-} is bound to Mg and chelated by a Na–N″–Na arm. The dimer has no crystallographic symmetry but is close to being C_2-symmetric. The average Mg–Se (2.3876 Å) and Na–Se (2.8357 Å) distance in **2** are slightly shorter than those in **1** (average values: Mg–Se 2.4141 Å, Na–Se 2.9438 Å). This is due to the fact that Se^{2-} is five-coordinate in **1** but only four-coordinate in **2**.

The thiohyponitrite complex **4** (Fig. 1d) crystallizes similarly to the hyponitrite complex **VIII**.[24] It encapsulates a *cis*-$SNNO^{2-}$ anion within an eight-membered Mg–Na1–N–Na3–N–Na4–N–Na2 ring and is bound by Mg–S, Mg–O, S–Na, O–Na and N–Na interactions The O–N–N–S bond distances in **4** are (Å): 1.357(1)–1.253(2)–1.730(1). The O–N and N–N distances in **4** are very much comparable to those in the hyponitrite anion in complex **VIII** (O–N: 1.363(2), N–N: 1.261(2) Å), implying that replacement of O for S hardly influences O–N and N–N distances. In contrary, comparing the O–N–N–S bond distances in **4**, 1.357(1)–1.253(2)–1.730(1), with those in a β-diketiminate Zn thiohyponitrite complex, 1.229(6)–1.306(7)–1.793(5),[35] shows significant differences that are likely related to differences between ionic bonding in **4** *versus* the more covalently bonding character in the Zn complex.

Computational studies

DFT calculations were conducted at the B3PW91-D3BJ/def2tzvp//B3PW91-D3BJ/def2svp level of theory which includes corrections for dispersion. The geometries for **1** and **3** have been optimized in C_2-symmetry. They are in agreement with

those obtained by X-ray diffraction and only minor discrepancies are noted. The calculated Ch–Na bond lengths (**1**: Na1 2.780 Å, Na2 2.986 Å; **3**: Na1/2 2.939 Å, Na3/4 3.132 Å) are slightly shorter than the experimentally found values (**1**: Na1 2.879 Å, Na2 3.008 Å; **3**: Na1/2 3.063–3.075 Å, Na3/4 3.214–3.226 Å).

Atoms-In-Molecules (AIM) analysis confirms bonding between Mg–Ch and Ch–Na through the identification of bond paths and bond-critical points (bcp's) along the Mg–Ch and Ch–Na axes (Fig. 2a and b). The electron density $\rho(\mathbf{r})$ in the Mg–Ch bcp's is 2–4 times larger than in the Ch–Na bcp's underpinning the observations of X-ray diffraction, that Mg–Ch is the prominent bond. However, the associated electron density $\rho(\mathbf{r})$ and Laplacian $\nabla^2\rho(\mathbf{r})$ in the bcp's are in all cases low, indicating a mainly ionic interaction. The Laplacian of the electron distribution shows a concentration of electron density at the Ch^{2-} centres which is mainly polarized towards Mg^{2+} and only weakly directed to the nearest Na^+ ions. The high electron density at the Ch^{2-} centres is further supported by Natural Population Analysis (NPA), which calculates a very low charge of −1.71 at Se and −1.64 at Te, and high positive charges at Mg (average +1.74) and Na (average +0.91), in line with ionic bonding between Ch^{2-}, Mg^{2+} and Na^+.

Fig. 2c shows the Laplacian and charge distribution for the thiohyponitrite complex **4**. The $SNNO^{2-}$ dianion is ionically bound in the metal crown with a total NPA charge of −1.75. The electron density on the Mg–S bond path is significantly smaller than that on the Mg–O bond path indicating that the Mg–O contact is the main bonding interaction.

Looking at the charge distribution within the thiohyponitrite anion (Fig. 2c) compared to that in the hyponitrite anion in **VIII** (Fig. 2d), it becomes clear that the latter has a major resonance form represented by $^-$O–N=N–O$^-$ whereas in thiohyponitrite there is charge delocalization: $^-$S–N=N–O$^-$ ↔ $^-$S–N$^-$–N=O. Both N atoms in $ONNO^{2-}$ are nearly neutral whereas the N atom next to S in $SNNO^{2-}$ carries a considerable negative charge.

Conclusion

The redox-active inverse crown complex **VI** is not stable in the presence of Me_3P=O. This is likely due to the high polarity of this phosphine oxide reagent which leads to loss of $(NaN'')_2$ from **VI**, resulting in $[(NaN'')(Me_3P{=}O)]_2$, which could be identified, and $[(BDI^*)Mg]_2Na_2$ which unselectively reduced Me_3P=O to a yet unidentified product. The much less polar heavier phosphine chalcogenides, R_3P=Ch (Ch = S, Se, Te), serve as excellent chalcogen transferring agents. Reduction of R_3P=Ch with the redox-active inverse crown **VI** led to inverse crown complexes with encapsulated Ch^{2-} dianions (**VII**-S, **1** and **3**). Choosing phosphine chalcogenides R_3P=Ch with R = Me or Et greatly simplified separation. Compared to solid PPh_3, the volatile phosphines PMe_3 and PEt_3 enabled high to quantitative product yields. Complex **VII**-S was previously prepared by reduction of S_8 with **VI**. However, a slight excess of elemental sulfur led to contamination of the sulfide product **VII**-S with the disulfide **VII**-S_2. Since excess of R_3P=S does not disturb the clean formation of **VII**-S, this is the preferred method of preparation. The heavier chalcogenides Se^{2-} and Te^{2-} are too large to be sufficiently stabilized by the tetrametallic $MgNa_3$-crown and required the formation of an extended pentametallic $MgNa_4$-crown. This was achieved by simple addition of 0.33 equivalents of $(NaN'')_3$ to the reaction mixtures. Reaction of $(BDI^*)MgNa_3N''_2(S)$ (**VII**-S) with N_2O in the presence of 0.33 equivalents $(NaN'')_3$ quantitatively yielded an inverse crown complex with the rare thiohyponitrite dianion *cis*-$SNNO^{2-}$. The high electron density is delocalized over the four heteroatoms and, apart from the $^-$S–N=N–O$^-$ resonance structure, features a significant $^-$S–N$^-$–N=O contribution. Current work focuses on expanding the scope of the reduce-and-capture properties of **VI** to other groups of the periodic table and various small molecules.

Conflicts of interest

The authors declare no competing financial interest.

Data availability

Supplementary information: synthetic procedures, selected NMR spectra, details for crystal structure determination, details for computational work. See DOI: **https://doi.org/10.1039/d5dt01896j**.

CCDC 2429354, 2429355, 2429356, 2387081 and 2449050 contain the supplementary crystallographic data for this paper.[40a–e]

Acknowledgements

We acknowledge A. Roth for CHN analyses, M. A. Schmidt for support with the computational part and Dr. C. Färber and J. Schmidt for assistance with NMR analyses. We thank the Deutsche Forschungsgemeinschaft for funding (DFG: HA 3218/12-1).

References

1 C. J. Pedersen, *J. Am. Chem. Soc.*, 1967, **89**, 7017–7036.
2 C. J. Pedersen, *Science*, 1988, **241**, 536–540.
3 C. J. Pedersen, *Angew. Chem., Int. Ed. Engl.*, 1988, **27**, 1021–1027.
4 A. R. Kennedy, R. E. Mulvey and R. B. Rowlings, *Angew. Chem., Int. Ed.*, 1998, **37**, 3180–3183.
5 R. E. Mulvey, *Chem. Commun.*, 2001, 1049–1056.
6 R. E. Mulvey, *Organometallics*, 2006, **25**, 1060–1075.
7 B. Li, C. Wölper and S. Schulz, CCDC 2290051. DOI: **10.5517/ccdc.csd.cc2gvzmy**.

8 S. Burnett, R. Ferns, D. B. Cordes, A. M. Z. Slawin, T. van Mourik and A. Stasch, *Inorg. Chem.*, 2023, **62**, 16443–16450.
9 P. Ghosh and G. Parkin, *Chem. Commun.*, 1996, 1239.
10 M. J. Evans, M. D. Anker, C. L. McMullin, N. A. Rajabi and M. P. Coles, *Chem. Commun.*, 2021, **57**, 2673–2676.
11 M. D. Anker and M. P. Coles, *Angew. Chem., Int. Ed.*, 2019, **58**, 13452–13455.
12 X. Zhang and L. L. Liu, *J. Am. Chem. Soc.*, 2023, **145**, 15729–15734.
13 W. A. Howard and G. Parkin, *J. Am. Chem. Soc.*, 1994, **116**, 606–615.
14 D. Rabinovich and G. Parkin, *Inorg. Chem.*, 1995, **34**, 6341–6361.
15 J. L. Kisko, T. Hascall and G. Parkin, *J. Am. Chem. Soc.*, 1997, **119**, 7609–7610.
16 C. Schneider, S. Ivlev and C. G. Werncke, *Eur. J. Inorg. Chem.*, 2023, **26**, e202200706.
17 W. Ren, G. Zi, D.-C. Fang and M. D. Walter, *J. Am. Chem. Soc.*, 2011, **133**, 13183–13196.
18 W. A. Howard, T. M. Trnka, M. Waters and G. Parkin, *J. Organomet. Chem.*, 1997, **528**, 95–121.
19 W. A. Howard and G. Parkin, *J. Organomet. Chem.*, 1994, **472**, c1–c4.
20 J. H. Shin and G. Parkin, *Organometallics*, 1994, **13**, 2147–2149.
21 J. H. Shin and G. Parkin, *Organometallics*, 1995, **14**, 1104–1106.
22 V. J. Murphy and G. Parkin, *J. Am. Chem. Soc.*, 1995, **117**, 3522–3528.
23 G. Giuffredi, T. Asset, Y. Liu, P. Atanassov and F. Di Fonzo, *ACS Mater. Au*, 2021, **1**, 6–36.
24 J. Maurer, L. Klerner, J. Mai, H. Stecher, S. Thum, M. Morasch, J. Langer and S. Harder, *Nat. Chem.*, 2025, **17**, 703–709.
25 R. D. Shannon, *Acta Crystallogr., Sect. A*, 1976, **32**, 751–767.
26 T. Chu, S. F. Vyboishchikov, B. Gabidullin and G. I. Nikonov, *Angew. Chem., Int. Ed.*, 2016, **55**, 13306–13311.
27 B. J. Reeves and B. M. Boardman, *Polyhedron*, 2014, **73**, 118–123.
28 S. M. Stuczynski, Y.-U. Kwon and M. L. Steigerwald, *J. Organomet. Chem.*, 1993, **449**, 167–172.
29 W. Imhof and G. Huttner, *J. Organomet. Chem.*, 1993, **448**, 247–253.
30 G. Hogarth, N. J. Taylor, A. J. Carty and A. Meyer, *J. Chem. Soc., Chem. Commun.*, 1988, 834–836.
31 D. Belletti, D. Cauzzi, C. Graiff, A. Minarelli, R. Pattacini, G. Predieri and A. Tiripicchio, *J. Chem. Soc., Dalton Trans.*, 2002, 3160–3163.
32 T. Chu, S. F. Vyboishchikov, B. M. Gabidullin and G. I. Nikonov, *Inorg. Chem.*, 2017, **56**, 5993–5997.
33 N. Sandblom, T. Ziegler and T. Chivers, *Can. J. Chem.*, 1996, **74**, 2363–2371.
34 H. Xu, A. Kostenko, C. Weetman, S. Fujimori and S. Inoue, *Angew. Chem., Int. Ed.*, 2023, **62**, e202216021.
35 N. J. Hartmann, G. Wu and T. W. Hayton, *Angew. Chem., Int. Ed.*, 2015, **54**, 14956–14959.
36 M. Á. Baeza Cinco, G. Wu, N. Kaltsoyannis and T. W. Hayton, *Angew. Chem., Int. Ed.*, 2020, **59**, 8947–8951.
37 B. Cordero, V. Gómez, A. E. Platero-Prats, M. Revés, J. Echeverría, E. Cremades, F. Barragán and S. Alvarez, *Dalton Trans.*, 2008, 2832.
38 D. E. Gindelberger and J. Arnold, *J. Am. Chem. Soc.*, 1992, **114**, 6242–6243.
39 D. E. Gindelberger and J. Arnold, *Inorg. Chem.*, 1994, **33**, 6293–6299.
40 (*a*) J. Maurer, L. Klerner, J. Langer, S. Harder, CCDC 2429354: Experimental Crystal Structure Determination, 2025, DOI: **10.5517/ccdc.csd.cc2mjy8d**; (*b*) J. Maurer, L. Klerner, J. Langer, S. Harder, CCDC 2429355: Experimental Crystal Structure Determination, 2025, DOI: **10.5517/ccdc.csd.cc2mjy9f**; (*c*) J. Maurer, L. Klerner, J. Langer, S. Harder, CCDC 2429356: Experimental Crystal Structure Determination, 2025, DOI: **10.5517/ccdc.csd.cc2mjybg**; (*d*) J. Maurer, L. Klerner, J. Langer, S. Harder, CCDC 2387081: Experimental Crystal Structure Determination, 2025, DOI: **10.5517/ccdc.csd.cc2l3ym9**; (*e*) J. Maurer, L. Klerner, J. Langer, S. Harder, CCDC 2449050: Experimental Crystal Structure Determination, 2025, DOI: **10.5517/ccdc.csd.cc2n6fmy**.